

Long-wavelength Radar Studies of the Lunar Maria

Bruce A. Campbell
Center for Earth & Planetary Studies, National Air and Space Museum

B. Ray Hawke
University of Hawaii

Thomas W. Thompson
Jet Propulsion Laboratory

Abstract

Radar measurements at 70 cm and 7.5 m wavelengths provide insight into the structure and chemical properties of the upper 5-100 m of the lunar **regolith** and crust. Past work has identified a number of anomalous regions and changes in echo strength, some attributed to differences in titanium content. There has been little opportunity, however, to compare calibrated **long-wavelength backscatter** among different units or to theoretical **model** results. We combine recent high-resolution (3-5 km) 70-cm radar data for the nearside with earlier calibrated full-disk observations to provide a reasonable estimate of the true lunar **backscatter** coefficient. These data are tested against models for quasi-specular scattering from the surface, echoes from a buried substrate, and Mie scattering from surface and buried rocks. We find that 70 cm echoes likely arise from Mie scattering by **distributed** rocks within the soil, consistent with earlier hypotheses. Returns from a buried substrate would provide a plausible fit to the observations only if the **regolith** depth were ~ 3 m or less and varied little across the maria. Depolarized echoes are due to some combination of single and multiple scattering events, but it appears that single scattering alone could account for the observed echo power, based on comparisons with terrestrial rocky surfaces. Backscatter strength from the **regolith** is most strongly affected by the loss tangent, whose variation with mineral content is still poorly **defined**. We compared the **backscatter** values for the mare deposits to the oxide contents inferred from spectral ratio methods, and found that in general the unit boundaries evident in radar images **closely** follow those seen in color difference

images. The 70-cm data are not well correlated with TiO_2 values found using the Charette relationship nor with Fe abundances derived from Clementine observations. The lack of a relationship between radar echo and Fe content is reasonable given the distribution of iron among various mineral phases, but ilmenite content (FeTiO_3) has typically been cited as the dominant cause of changes in loss tangent (and thus the radar absorption). The lack of correlation between the radar data and TiO_2 estimates may arise from uncertainties in the Charette technique, subtle differences in the upper surface and bulk properties of the regolith, mineralogic effects on the radar not linked to titanium content, or to some combination of these factors. Dark crater haloes in the mare and highlands, and low radar returns from apparent cryptomare regions, are used to illustrate the role radar data can play in identifying changes in regolith composition; low-return haloes around craters such as Petavius may indicate 5-25% contamination of the highlands soil by excavated mare material or a layer of rock-poor ejects at least several meters deep. The 7.5-m data were shown to correlate to a reasonable degree with estimates of Fe abundance, suggesting that this component of the mare basalts is primarily responsible for attenuation losses at very long wavelengths. The different sensitivities of the two radar wavelengths and multispectral data offers the potential for future deep mapping of the mare lava flows and regolith.

Introduction

The composition and structure of the lunar regolith are of fundamental importance to the geologic study of the Moon. The regolith is a mixture of fine soil particles, small blebs of glass (agglutinates), and a variety of rock fragments, all formed by impact bombardment, which overlies the bedrock lava flows in the maria and basin-produced layering in the highlands. The majority of the included rocks are locally derived from the bedrock underlying the regolith, but some fraction are transported from distant areas by large impacts. The regolith layer is estimated to be 3-8 meters deep in the mare areas [Horz et al., 1991]. In vertical section, the regolith is a complex assortment of thin layers produced by impact craters and subsequent micrometeorite gardening. Over large

areas, it is expected that these layers are not coherent, and that any stratification in the soil is localized and highly variable,

Apollo core samples, seismic data, and the lunar sounder experiment characterized some of the physical bounds on regolith depth and grain size, but the variability of soil properties across the Moon is not entirely understood. Most of the compositional information for these soils comes from spectral ratio parameters and orbital geochemistry data which have been calibrated to measured values for the Apollo and Luna sample sites. The primary interest in remote mare soil studies is a determination of their bulk oxide content, which is dominated by FeO, TiO₂, Al₂O₃, MgO, and CaO (excluding the silica component) [Papike et al., 1991]. These oxides are found in minerals such as olivine, pyroxene, and ilmenite, and vary across the maria due to lateral differences in magma source regions and fractionation histories. Knowledge of the abundance of these oxides thus provides a clue to the formational history of the upper lunar crust.

Radar scattering from the regolith can come from several sources, whose importance varies with the wavelength, λ , of the probing energy. Surface rocks and regolith sculpture will be the primary scatterers at X-band wavelengths (3 cm), while larger blocks and those buried in the soil become progressively more important at S (12 cm) and P (70 cm) band. Finally, any strong dielectric boundary, such as between the soil and a rock basement, will make a contribution if the radar energy is not attenuated prior to encountering the bedrock interface. Imaging radar data for the Moon have often been used as a tool for characterizing the regolith, particularly in the study of crater ejecta distribution and large pyroclastic deposits [e.g., Zisk et al., 1977; Thompson et al., 1979; Moore et al., 1980; Gaddis et al., 1985]. Much of this work utilized the 3.8-cm radar maps of Zisk et al. [1974], whose 2-km resolution and sensitivity to surface roughness delineated numerous subtle features. The 70-cm data typically were of much lower spatial resolution, but significant gains were made in identifying echo sources and the role of regolith properties.

Schaber et al. [1975] determined that the lava flows mapped in Mare Imbrium, which varied widely in their TiO₂ abundance, showed a strong degree of correlation with unit boundaries in the 70-cm data available at the time (5-10 km resolution), and that higher titanium abundances are

linked to lower radar echo strength. Work by Thompson et al. [1970] and Pollack and Whitehill [1972] led to a consensus that the 70-cm radar echoes came largely from rocks buried within the fine soil of the regolith, and that changes in the backscatter strength were due to shifts in the loss tangent of the dust. The loss tangent, in turn, was linked to the oxide content of the material, and lab studies of returned samples (summarized in Carrier et al. [1991]) appeared to confirm these theories. To date, however, there have been no efforts to test the 70-cm data as a possible Moon-wide mineralogic mapping tool, and questions as to the source of the echo power remain. To a large degree this work was hampered by a lack of calibrated data for the entire nearside, but the 3-5 km resolution map of Thompson [1987] overcame this problem using a low-resolution beam-swing technique. The 7.5-m data have been discussed only in the original report by Thompson [1978], which presented models to show that the primary echoes were coming from rock layers beneath the regolith.

The spectral reflectance of the lunar soil is controlled by the mineralogy of the original material, the degree of maturation (agglutinate formation), and by the degree of contamination of the surface layer by impact debris from other geologic targets. Since the depth of penetration for reflected visible/IR energy is only a few microns, surficial effects dominate the observed spectrum. A number of methodologies have evolved to provide estimates of oxide content from this type of remote sensing data. The earliest application of color variability in soils was carried out by Whitaker [1972], who showed that a red-blue ($0.37/0.61 \mu\text{m}$) difference image suppressed albedo changes and revealed geochemical variations within the maria [see also Wilhelms, 1987]. Charette et al. [1974] found that the $0.40/0.56 \mu\text{m}$ ratio for mature mare units correlated with the TiO_2 abundance defined from returned samples, and proposed an empirical model for extending this relationship to other mature mare soils. Subsequent analysis by Pieters [1978] used 4 major criteria, including the Charette ratio, to map basalt units on the Moon into about a dozen categories. The utility of this method in areas of lower TiO_2 abundance suffers due to a progressively wider spread in the possible ratio values in this range and a sensitivity to other regolith components such as iron [Pieters, 1978; Johnson et al., 1991; Pieters et al., 1993; Melendrez et al., 1994]. The

constraint on soil maturity is very strict, since immature mare material or highlands contamination will have a major impact on the $0.40/0.56 \mu\text{m}$ ratio. Johnson et al. [1991] mapped the TiO_2 values for the lunar nearside using the Charette relationship at a resolution of $\sim 1 \text{ km}$, and the digital versions of these maps are used here. A method for determining iron abundance from Clementine 750 and 950 μm data, which includes the effects of soil maturity, has been developed by Lucey et al. [1995], and their 30-km resolution maps will also be used as a comparison to the radar data. The Apollo gamma ray spectrometer data have been used to estimate Fe and Ti bulk abundances [Davis, 1980], but the spatial coverage and resolution of these maps is rather low ($\sim 100 \text{ km}$).

An interesting aspect of the radar data is the fact that they depth-average the properties of the regolith over a significant path length (up to 10 wavelengths or more). Where a thin layer of immature soil or highland contaminant (a crater ray, for example) can drastically affect the spectral reflectance of a surface, to the long-wavelength radar this constitutes a small fraction of the total volume which contributes to the echo. This difference in sensitivities suggests that the optical and radar data can offer complementary information. Past work has shown that the 70-cm observations may be a useful tool for mapping the bulk composition of the regolith, but significant issues in the nature of the scattering need to be addressed. In this paper, we first examine possible sources for the long-wavelength backscatter, and compare the observational data with theoretical models to constrain the range of potential regolith structure. We then compare the 70-cm and 7.5-m data to spectral-ratio methods for oxide mineral mapping. Finally, we present examples of the role long-wavelength radar data can play in characterizing the lunar regolith, and discuss the types of future observations which may address outstanding problems.

Analysis of 70-cm Scattering

The 70-cm maps used here, which have a spatial resolution of 3-5 km, were collected in 1986 at Arecibo Observatory, and are shown in Figure 1. In contrast to previous mosaics at this wavelength, which were hampered by a lack of calibration between individual images, the current

image was assembled using a low-resolution beam-swing technique to provide a global reference map for radar brightness [Thompson, 1987]. To compare these data to the results of theoretical models, we first calibrated the radar images to values of backscatter cross section per unit area (σ_0). This was done by letting the mean polarized (LR: left-circular transmit, right circular receive; also called opposite-sense circular or OC) echo behavior at 70 cm be characterized by the 68-cm lunar average compiled by Hagfors [1970]. The depolarized (LL: left-circular transmit, left-circular receive; also called same-sense circular or SC) returns were calibrated by letting the average echoes near the limb be 1/2 (-3 dB) the strength of the polarized component, again as indicated by earlier disk-integrated measurements [Hagfors, 1970]. The systematic error in these calibrations is difficult to define, but mosaicking offsets probably produce error bounds of about 1-2 dB between sites in widely separated locales.

The 70-cm radar echoes are influenced to varying degrees by (1) the volumetric rock population, (2) regolith depth, (3) substrate presence and roughness, and (4) the dielectric properties of the rocks and fine soil. To examine the effects of these parameters, we study three sources of radar returns: quasi-specular echoes from the upper surface of the regolith, echoes from a buried substrate, and Mie scattering from surface and buried rocks.

Quasi-specular Scattering. This component, assumed to arise from single scattering facets which are large with respect to the radar wavelength, contributes only to the polarized (LR) echo power. Using the model of Hagfors [1964], we can predict the backscatter coefficient for a typical lunar surface reflectivity of 0.07, corresponding to a real dielectric constant (ϵ') of 3 (Figure 2). Tyler [1979] found that mare surfaces can be described by rms slopes (γ) of $\sim 20^\circ$ for radar wavelengths around 1 m, while highland areas can have rms slope values of 4-70. For incidence angles of $>10^\circ$, the Hagfors model (with $\gamma=20^\circ$) underestimates the average lunar backscatter by at least 3 dB, indicating that a significant portion of the polarized echo is coming from diffuse scattering by surface or buried rocks. Significant changes in rms slope or Fresnel reflectivity (e.g., real dielectric constant) between the maria are unlikely [Tyler, 1979], so we expect that the quasi-specular

mechanism does not contribute much to the variability in mare radar echoes for incidence angles above -20° .

Buried Substrate Model. This model assumes that a significant portion of the echo comes from a buried scattering layer, characterized by the transition from soil to rock, whose depth and roughness vary. In this end-member scenario, no scattering rocks are present in the soil. The substrate could have a range of scattering behaviors depending upon its roughness, but our primary interest here is in the backscatter response of such a model for changes in the microwave loss factor. The loss tangent is defined as the ratio between the imaginary and real components of the complex dielectric constant: $\tan\delta = (\epsilon''/\epsilon')$. The amount of power lost in passing twice through a layer with a given complex dielectric constant is:

$$P(h) = P_0 e^{-4 \alpha h / \cos\theta} \quad (1)$$

where the loss factor is

$$\alpha = \frac{2\pi}{\lambda} \left[\frac{\epsilon'}{2} \left[\sqrt{1 + \tan^2\delta} - 1 \right] \right]^{0.5} \quad (2)$$

P_0 is the incident power at the surface, h is the depth of the layer, λ is the radar wavelength in vacuum, and θ is the incidence angle within the absorbing layer:

$$\theta = \sin^{-1} \left[\frac{\sin\phi}{\sqrt{\epsilon'}} \right] \quad (3)$$

with the radar incidence angle at the surface given by ϕ [Ulaby et al., 1987]. Transmission effects at the top of the soil layer also reduce the observed backscatter. We estimate the loss factor for a circular-polarized wave as the average of T_h and T_v , the H- and V-polarized Fresnel transmission coefficients (i.e., one-half the power is present in each of the two linear polarizations) [Stratton, 1947]:

$$T = \frac{T_h + T_v}{2} = \frac{\sin 2\phi}{2 \sin^2(\theta + \phi)} \frac{\sin 2\theta}{\sin^2(\theta - \phi) \cos^2(\phi - \theta)} \quad (4)$$

and for the two-way case of a buried layer this factor must be squared, The polarization effects of the interface due to differences in T_h and T_v are neglected in this treatment. Given the scattering cross-section of a buried layer, we can thus estimate the observed backscatter after allowing for transmission and absorption. The effect of a reduced dielectric contrast at the soil-rock interface relative to that between the rock and free space would most likely be to further lower the effective cross section of the substrate.

The electrical properties of rocks have been studied in detail by a variety of measurement techniques, with good summaries provided in Ulaby et al. [1989] for terrestrial samples and by Carrier et al. [1991] for lunar rocks. In general, the real part of the dielectric constant is dependent upon rock density, p , with little variation due to oxide content. Lunar soils have real dielectric constants of ϵ' from 2-3, while solid rocks may have values of ϵ' from 4-8 depending upon their porosity. The imaginary part of the dielectric constant for dry samples is affected by bulk chemistry, with little influence noted for changes in sample density [Ulaby et al., 1989]. For lunar materials, $\tan\delta$ is found to vary by an order of magnitude, from about 0.002 to 0.02, with increasing (FeO+TiO₂) values. Olhoeft and Strangway [1975] derived a power-law relationship between oxide content, density, and loss tangent at 67 cm wavelength:

$$\tan\delta = 10^{(0.033[\%TiO_2 + \%FeO] + 0.231 p - 3.061)} \quad (5)$$

These results have scatter of up to an order of magnitude in $\tan\delta$, so the reliability of the best-fit equation is tenuous, and we have no certainty that the influence of oxide content on $\tan\delta$ is accurately modeled,

The change in backscatter strength for a mantled scattering surface is shown in Figure 3 for layer depths of 3-8 m and the expected range of loss tangents. From these results, we can conclude that the range in backscatter of a buried layer with changes in either h or $\tan\delta$ is quite large. At layer depths of more than about 3 m, this range in brightness with loss tangent would exceed that observed (about 8 dB, or a 6:1 ratio) across all of the nearside maria, For shallower depths, the backscatter would strongly reflect the character of the underlying flows (buried craters, changes in

roughness, etc.) and minor variations from the average thickness. It is uncertain to what degree the regolith depth and substrate roughness might be similar over large regions of the Moon, but any changes in these parameters would tend to create variations in the backscatter strength that would not be correlated with the chemical changes responsible for color differences. For deeper regoliths, the attenuation would be strong enough to “hide” all but very rough buried surfaces. While we cannot rule out substrate echoes entirely, they seem unlikely to form a major component of the observed return.

Mie Scattering from Roth. Another end-member model describes the regolith as a collection of rocks randomly distributed through a layer of given depth. These rocks are further distributed in size according to a power-law relationship. A first-order estimate of the polarized backscatter cross section can be obtained by using Mie theory, assuming that only single scattering is important and neglecting shadowing of one rock by others [Bohren and Huffman, 1983]. Thompson et al. [1970] and Pollack and Whitehill [1972] tested the Mie scattering mechanism and concluded that returns from buried rocks were likely a major component of the 70-cm radar echoes, but they lacked calibrated data to carry the analysis to a local level. They further suggested that the primary cause of changes in the echoes was chemical (i.e., $\tan\delta$) variations in the regolith, and that such changes could be used for geological mapping. The Pollack and Whitehill study also treated multiple scattering, and found that the average radar cross section and degree of polarization for the Moon could be modeled by a reasonable rock distribution. Their model is rather complicated in assuming that rocks are primarily found in concentric regions around parabola-shaped fresh young craters, but it ignores any depolarization by single scatter from non-spherical objects, doesn't treat the issue of regolith variations within a crater cavity, and takes a single rock population from the Tycho ejects blanket as its test case. In this paper, we will examine just the Mie single-scattering model and compare its results to the calibrated 70-cm observations for the Surveyor landing sites.

The difference between the Mie scattering case and the substrate model discussed above is in the effect of the loss tangent on the echo. For a population of rocks randomly distributed in size

throughout the layer, the net effect is to average the absorption over the **total** depth rather than to integrate along the large total path length from the surface to a buried substrate. We can write the total backscatter cross section as:

$$\sigma_o = \frac{T^2}{4\alpha} [1 - e^{-4\alpha h / \cos\theta}] \int_{r_{min}}^{r_{max}} \sigma(r) p(r) dr \quad (6)$$

$p(r)$ is the population density of rocks with radius r (in number/m³), $\sigma(r)$ is the scattering cross section (m²) for each rock derived from the Mie equations, and R_{min} and R_{max} are the range of rock sizes likely to produce 70-cm scattering (we integrate from 1 cm to 2 m). Note that the effect of h on σ_o in Eq. 6 is entirely contained in the exponential term, which disappears for large optical depths,

Rock populations for the lunar **regolith** are available from work done on the Surveyor **landing** site images by Shoemaker and Morris [1968], which were converted to differential probability functions by Thompson et al. [1970]. Volumetric populations can be obtained by equating the fractional area covered by surface rocks and the fractional volume occupied by buried rocks ("Rosival's Principle", discussed by Shoemaker and Morris [1968]). From this approach, the differential volumetric rock population can be found from the surface distribution as:

$$p(r) = \frac{3}{4} C_s r^{-n} \quad (7)$$

where C_s is the coefficient of the surface differential rock power law, and n is the exponent. Table 1 lists the best-fit rock populations for the Surveyor sites, showing that regions within the maria (all but Surveyor 7) can vary significantly in their behavior, presumably due to the relative proximity of young craters to each landing site. This table also includes the measured cross sections for each site from the calibrated 70-cm map.

We calculated the total **Mie** surface **backscatter** cross section for each Surveyor site and found that, even with a strong **rock/soil** dielectric contrast, more surface scattering is at least 6 **dB** weaker than the observed echo strength (Table 1). Only if the loss tangent of the rocks is allowed to drop to values of -0.001 (where internal reflections within the rocks become very efficient) can we

replicate the observed polarized cross section, and such low loss factors seem plausible only for anorthositic highlands material. Figure 4 shows the echoes found for volume scattering from Eq. 6 and the populations in Table 1, and demonstrates that even a low rock/soil dielectric ratio ($\epsilon'_r = 5$, $\epsilon'_s = 3$) and regolith depth of 5 m can produce echoes consistent with the 70-cm polarized observations. Both results are in accord with those of Thompson et al. [1970], but it appears that multiple scattering is not necessarily required to produce the measured polarized echo.

The depth of the rock-filled layer is important to the results of the **Mie** modeling. At loss tangents above -0.01, the regolith appears to the 70-cm radar to be “bottomless” (infinite optical depth) for thicknesses of 5 m or more (Fig. 4). With lower loss tangents or thin regolith layers, the effect of changes in depth on the observed return becomes very large. At the same time, these conditions favor echoes from the buried soil-rock interface. We have the same situation here as for the substrate model above: if the regolith were thin enough to exhibit wide swings in backscatter with small changes in depth (i.e., $h < 5$ m), then we would expect these variations to be uncorrelated with the chemical changes in the maria. Since the radar and color-difference boundaries tend to match well, this argues for the deeper regolith.

Depolarization. The depolarized component can be attributed to some combination of transmission effects through a dielectric interface (i.e., the soil surface), single-scattering by non-spherical objects, and multiple scattering between rocks suspended in the soil [Hagfors, 1967]. The first mechanism is not very efficient, and at most produces only a few percent ellipticity in the received signal. The latter two mechanisms have the potential to produce significant depolarization, with the extreme case being that of randomly oriented small linear objects, which produce equal LL and LR returns. Polarization ratios (LL/LR) in the maria range from 0.05 to 0.40, increasing with incidence angle as the quasi-specular component of the LR return becomes less significant. Near the limb, Hagfors [1970] noted that the ratio was about 0.5, a fact we used for calibration purposes.

Pollack and Whitehill [1972] showed that multiple-bounce radar returns can be a significant part of the total echo if the rock population is high, such as in a crater ejecta blanket. It is difficult to judge the relative contributions of single and multiple scattering to the depolarized echo, however, since the shape of the rocks and the pattern of scattered radiation play a major role. The LL/LR values noted above and their progression with incidence angle match the trends observed for terrestrial rocky surfaces at 68-cm wavelength (Figure 5), for which we anticipate little multiple scattering. Single-scattering may thus be capable of producing the observed amount of lunar depolarization. In general, however, the total return should be a sum of many scattering events whose paths through the regolith and single-scattering albedoes (dependent mostly upon the real dielectric contrast) do not change with soil $\tan\delta$. As such, we expect the multiple" scattered component to scale linearly with the change in single-scattered energy.

Summary. The variations in 70-cm radar echo from the lunar mare are dominated by changes in the scatter from rocks buried in the soil. Significant contributions from a buried substrate are likely only in the extreme case of a very low soil loss tangent, a thin soil layer, a very rough substrate, and small rock/soil dielectric contrasts. Note that this last constraint will further reduce the substrate echo, so the net gain for such changes is slight. Echoes from buried surfaces are likely to be important only in 70-cm scattering from relatively rock-free layers such as pyroclastic deposits. A large component of subsurface Mie scattering is **also** consistent with the 12.6-cm lunar radar studies of Stacy [1993], who found that the echo from buried objects must be stronger in the polarized (LR) sense than in the depolarized mode.

There is a strong dependence of **backscatter** on the microwave loss tangent in all situations, and a sensitivity to **regolith** depth changes which depends upon the average thickness of the layer. If the region of mixed rocks and fine soil is less than 5 m deep, then we expect major shifts in backscatter power for **small** changes in layer thickness and substrate roughness. Since neither effect will be linked with the mare lava flow chemistry, such changes would tend to blur or eliminate the correlation between radar and color-difference boundaries. Given the close agreement

between these unit boundaries, we conclude that a deep-regolith scenario (5 m or more) is a reasonable assumption.

Changes of 3 dB or more are possible in the Mie model for reasonable shifts in the real dielectric constant (i.e., the density) of the buried rocks ($\epsilon' = 5-7$), but over the maria we can likely choose a single mean value for rock density which will not vary systematically from one basalt flow unit to the next. Measured variations in rock population are quite large among the Surveyor I, III, V, and VI sites, leading to a 5-8 dB range in predicted radar volume scattering. The lack of a similar large shift in the observed echoes from the various sites (Surveyor V is actually slightly brighter relative to the lunar mean than Surveyor I) suggests that the local rock counts do not indicate regional differences in regolith structure, but rather the proximity of young craters to the landing sites. For the large pixel size (3-5 km) of the current 70-cm data, a single average rock population for the mature mare areas away from large fresh craters **seems** appropriate. Some doubt exists in this assumption, based on the infrared eclipse brightness temperatures **found** for the mare surfaces by **Shorthill** [1973], The **Imbrium** and **Procellarum** lava flows have higher eclipse temperatures than the older **Serenitatis** and **Tranquilitatis** materials, **suggesting** a higher surface population of rocks or a more granular particulate surface soil [Moore et al., 1980]. These differences are not evident in the 3.8-cm radar mosaics [Zisk et al., 1974], which argues that the changes in mare rock population are not as significant as variations in the loss **tangent**.

Given the above results, we can ascribe the large variations in 70-cm **backscatter** in the maria to changes in the loss tangent of the fine soil. This **link** will be best for the depolarized echo, which is free of surface quasi-specular contributions, Multiple scattering effects should scale with loss tangent in the same manner as the single-scattered echoes, so an exact knowledge of the relative contributions from the two mechanisms is **unnecessary**. Depolarized scattering from a substrate will also be weaker than the polarized return due to the lack of quasi-specular returns, so our concerns about such contamination of the observed echo should be minimized.

The models discussed above suggest that most depolarized radar echo changes can be attributed to loss tangent variations. Laboratory work has shown a positive correlation between TiO_2 and FeO content and $\tan\delta$, so the next step is to compare the observed backscatter with estimates of mare basalt mineralogy. We chose 30 sites in the lunar maria which show the range of echo strengths across these units (Figure 1). Each site was selected to sample only one type of basaltic unit as defined by Pieters [1978] and to avoid the ejecta blankets of large craters. The LR and LL echoes for these sites are plotted in Figure 6 with the lunar mean and the P-band AIRSAR σ_0 data for four Hawaiian lava flows added for reference. [Campbell et al., 1993; Campbell and Campbell, 1992]. Note that while nearly all the mare sites fall below the lunar mean, a few areas have notably higher backscatter. For the mare test sites, we plotted the polarized and depolarized echo enhancements (differences from the lunar mean; Figure 7). It is clear that the enhancements in the two polarization modes are closely related, which suggests that the primary source of changes in the echo at incidence angles $>25^\circ$ is variability in diffuse scattering, and that the percentage of depolarization does not vary with location or soil properties (i.e., the rocks tend to have a similar distribution of shapes and sizes across the maria). The LL/LR values for the mare sites fall in the range of very smooth terrestrial surfaces (Figure 5). This again suggests that single-scattering alone could produce the observed depolarization.

Comparison of 70-cm depolarized radar backscatter values, corrected for a cosine dependence of projected area on incidence angle, to Fe abundance from Lucey et al. [1995] shows no correlation whatever (Figure 8). The lack of a link between the Fe map and the radar echo is not surprising, since iron content has no systematic variation with oxide mineral abundance in lunar basalts [Papike et al., 1991]. Evidently the free iron in regolith agglutinates, which we expect would interact strongly with the microwave energy, either does not vary in a significant way among the maria or has too low a concentration to affect the radar absorption.

A similar comparison to the TiO_2 values of Johnson et al. [1991] yields the weak negative correlation also shown in Figure 8. At best the titanium abundance defines an upper limit for the

radar echoes, but there is a wide spread in the returns, particularly at TiO_2 values below -4%. It has long been held that variation in ilmenite (FeTiO_3) content is the primary factor in radar absorption in the mare regolith [Pollack and Whitehill, 1972]. The broad correspondence between titanium content (defined from the Charette method) and radar echoes noted by Schaber et al. [1975] for Mare Imbrium lava flows near Carlini crater still holds, and the low-Ti basalts in Mare Serenitatis do have high radar returns. The relationship, however, does not hold well for maria such as Crisium and Fecunditatis, which have much lower radar returns than their TiO_2 values might imply. Mare Fecunditatis is especially odd, with the lowest echoes of any major mare surface despite the classification of its northern half by Pieters [1978] and Wilhelms [1987] as a medium- TiO_2 region. The southern half is classified by Wilhelms as complex or undivided, perhaps due to the large influence of Langrenus crater ejecta on the spectral reflectance properties of this region. Mare Tranquilitatis, whose western half has the highest TiO_2 estimates on the nearside (9% or more [Johnson et al., 1991; Melendrez et al, 1994]), is intermediate in radar echo strength.

These results suggest several possible scenarios: (1) the loss tangent is dependent upon the TiO_2 content, but the Charette relationship has large errors for low-Ti units [Pieters et al., 1993], (2) the surface and sub-surface composition of the regolith are, different, leading to discrepancies in the inferred amounts of titanium, (3) other mechanisms are responsible for changes in $\tan\delta$. There is no evidence to support the second hypothesis, so it is likely that both (1) and (3) contribute to the observed scatter in the data. Improvements in the determination of titanium content using Clementine data should provide a better test for the link between this regolith component and radar backscatter, while the search for other mineralogic effects on $\tan\delta$ may require additional lab studies of lunar samples.

Despite the uncertainties in directly interpreting 70-cm backscatter in terms of microwave loss tangent, there are numerous opportunities for complementary use of these data and multispectral images. Throughout the maria, craters occur with haloes of low 70-cm radar return (Table 2, which expands on a list compiled by Thompson [1974]). These haloes extend 1-2 crater diameters from the rim, outboard of a zone of radar-bright rough ejects which varies in width between craters; in some instances the radar-dark halo reaches the rim of the crater. The low-return area may indicate the presence of more absorbing (higher $\tan\delta$) material within the soil layer. This higher $\tan\delta$ component in turn implies a more absorbent layer of basalt present somewhere in the underlying lava flow units. Radar-dark haloes also exist for craters within the highlands, most often near the boundary of the mare and terra surfaces. Aristarchus [Guest and Spudis, 1985; McEwen et al., 1994] and Petavius are good examples of highland crater anomalies (Figure 9), but there are several other large craters which have similar dark haloes (Table 2). Excavation of mare basalt and its incorporation into the highland **regolith** by craters near mare edges is a plausible explanation for these haloes, since the mixed **regolith** would have a lower total radar echo than pure highlands material. In both cases, a relatively **block-free** mantling deposit could also potentially account for the observed low radar return [Oberbeck, 1975].

We examined first the question of how much mare material is required to change the observed highland back scatter by using the Mie scattering model (Eq. 6). For large optical depths, the change in **backscattered** power scales with the shift in a for the original and mixed soils. The loss factor in turn changes with $\tan\delta$, and we have treated this factor as a linear combination of the loss tangents for the two **regolith** components. Lab results for Apollo samples show that highland $\tan\delta$ values may be as low as 0,001, and mare soils may vary from 0.002 to 0.02 [Carrier et al., 1991]. Figure 10 shows the loss in **backscattered** power as a function of mare contaminant fraction for this range of values. For Petavius, the nearby highlands are 3-5 dB brighter than the dark halo surrounding the crater. This implies a 5-10% level of mare contamination **within** the halo for a highly absorbing basalt component, and 12-25% contamination by a more intermediate mare material ($\tan\delta=0.01$).

If the same anomalies were due to rock-free ejects superposed on the normal regolith, then a modification of the Mie model yields the power lost as a function of the depth, h' , of the mantling layer:

$$\frac{P_{\text{mantled}}}{P_{\text{unmantled}}} = e^{-4 a h'} \{ \cos\theta \} \quad (8)$$

where we have again assumed an infinite optical depth for the underlying normal regolith. The plots in Figure 11 show the power loss for three values of the regolith loss tangent; the effect of a surficial mantling layer is most dramatic for very lossy deposits. The 3-5 dB change in the Petavius halo would require a mantle more than 3 m deep for a low-loss material typical of the highlands. Based on McGetchin et al.'s [1973] model for ejects depth as a function of distance from the rim, Petavius could have emplaced up to 35 m of material at the margins of the observed halo (~150 km from the rim crest). In such a case, the observed drop in backscatter could be obtained with simply a lower volumetric rock density over the depth of the ejects, rather than by an idealized rock-free mantle. For haloes in the maria, significant power drops require a mantle depth of 1 m or more, which again are not unreasonable for the crater sizes involved.

In addition to the low-return crater haloes, there are regions where cryptomare materials which have been covered by later basin ejects are evident from the low radar return produced by mixing of basalt and anorthositic material (i.e., the Schiller-Shickard region and areas northwest of Mare Humorum shown in Figure 12) [Hawke et al., 1993]. Multi-spectral methods have been used to study dark-halo craters and regional cryptomare deposits, and to infer the nature of the buried material [Bell and Hawke, 1981; Head et al., 1993], but these approaches have difficulty characterizing such mixed terrains in the presence of rays and other ejects which often dominate the surface reflectance. The long-wavelength radar data may offer a complementary tool for inferring the boundaries of buried mare terrain, and the same techniques discussed above will allow estimation of the degree of basaltic contamination in these areas.

Analysis of 7.5 m Radar Data

The 7.5-m wavelength radar image (LR polarization only) was collected in 1977 at Arecibo Observatory, and has a resolution of 30-50 km [Thompson, 1978]. Since the original data were unavailable, the map was recovered by digitally scanning a photo negative and putting the image into a cartographic framework (Figure 13). The registration of the radar image and base map are relatively good near the center of the Moon, but there are positional errors near the limbs, so we did not attempt any reprojections of the data. The very long radar wavelength will penetrate a considerable distance into the sub-regolith basalt, and the paucity of scatterers within the regolith at the wavelength scale means that the soil/rock layer plays little role in the final return. For the maria, these data thus reflect the scattering and absorption properties of the basalt layers below the soil. Penetration and scattering within rocky surfaces was inferred from 68-cm AIRSAR data for Hawaii [Campbell et al., 1993]; the ten-fold increase in wavelength and the absence of water should greatly enhance this mechanism for the lunar 7.5-m observations.

The behavior of the 7.5-m data for the maria is often not well matched with the 70-cm results. Mare **Serenitatis**, seen at 70 cm to be one of the brightest mare surfaces, has very low 7.5 returns in the southwestern half of the basin. This contrasts with the echoes from Mare **Tranquilitatis**, which despite its high TiO_2 content and low 70-cm echoes is the brightest mare at 7.5 m. Mare **Fecunditatis** and Mare **Crisium** have intermediate 7.5-m backscatter, whereas **Fecunditatis** has the lowest 70-cm returns of any large mare. The lowest 7.5 m echoes on the Moon are associated with the **Imbrium**, **Humorum**, and **Procellarum** mare deposits

Mare behaviors at 7.5 m wavelength correlate qualitatively with the iron abundances inferred from **Clementine** data [Lucey et al., 1995]. **Imbrium**, **Procellarum**, and **Humorum**, all characterized by low radar returns, have the highest levels of Fe. **Crisium** and **Fecunditatis**, which have the lowest iron contents, have higher 7.5-m echoes. This correlation is not ideal, since the high radar returns for **Mare Tranquilitatis** are matched by only intermediate iron values. It does appear,

however, that iron abundance has a stronger effect on the mare 7.5-m radar return than was observed at 70 cm.

Conclusions

Analysis of scattering models for the lunar regolith showed that most variations in depolarized radar backscatter can be attributed to changes in the microwave loss tangent, provided the depth of the soil/rock layer is 5 m or more. Thinner layers will have significant substrate echoes and a strong dependence of echo strength on minor changes in thickness. Since these changes would not be correlated with the geochemical properties of the mare basalts, we would expect such a situation to destroy the observed strong correlation between radar and color-difference unit boundaries. Use of the depolarized radar echo also avoids possible surface and subsurface quasi-specular scattering components.

In general the 70-cm depolarized radar backscatter cross section does not correlate well with either the TiO_2 abundances calculated from the Charette relationship or the Fe values estimated by Lucey et al. [1995] from Clementine data. The TiO_2 values at best define an upper limit on the radar echo strength. These results suggest that the Charette relationship has a wide error range at low TiO_2 values, the radar echo is sensitive to other components of the regolith, or some combination of these effects. The 7.5-m data were shown to correlate to a reasonable degree with estimates of Fe abundance, suggesting that this component of the mare basalts is primarily responsible for attenuation losses at very long wavelengths. Analysis of radar-dark crater haloes leaves open the possibility of either excavated mare material or rock-poor ejecta deposits. Further analysis and correlation with the results of spectral mixture models for these areas are required to discriminate between the two scenarios.

Future work will focus on better calibrating the 70-cm radar echoes to oxide abundances and on the investigation of anomalous regions. Observations at this wavelength with resolutions as fine as 300 m are possible from Arecibo, so new work will be carried out to image areas of particular

interest. These data provide a valuable complementary tool to multi-spectral techniques, and it is expected that much can be gained from their synthesis.

Acknowledgments

The authors thank Haig Morgan at the USGS for scanning the 7.5-m radar image, Jeffrey Johnson for providing the digital TiO₂ maps, and Paul Lucey for digital versions of his iron maps. Thanks also to Ted Maxwell for helpful comments. This work was supported in part by NASA PG&G grant NAGW-3360 (B. A.C.). The research conducted by T. W. I. was performed at the Jet Propulsion Laboratory, California Institute of Technology, under a contract with NASA.

References

- Bohren, C. F., and D.R. Huffman, Scattering and emission from small particles, John Wiley, NY, 1983.
- Campbell, B. A., R.E. Arvidson, and M.K. Shepard, Radar polarization properties of volcanic and playa surfaces: Applications to terrestrial remote sensing and Magellan data interpretation, *J. Geophys. Res.*, 98, 17099-17114, 1993.
- Campbell, B. A., and D.B. Campbell, Analysis of volcanic surface morphology on Venus from comparison of Arecibo, Magellan, and terrestrial airborne radar data, *J. Geophys. Res.*, 97, 16293-16314, 1992.
- Carrier, W. D., G.R. Olhoeft, and W. Mendell, Physical properties of the lunar surface, in@ Sourcebook, Cambridge Press, New York, 1991.
- Charette, M. P., T.B. McCord, C. Pieters, and J.B. Adams, Applications of remote spectral reflectance measurements to lunar geology classification and determination of titanium content of lunar soils, *J. Geophys. Res.*, 79, 1605-1613, 1974.
- Davis, P. A., Iron and titanium distribution on the Moon from orbital gamma ray spectroscopy with implications for crustal evolutionary models, *J. Geophys. Res.*, 85, 3209-3224, 1980.
- Gaddis, L. R., C.M. Pieters, and B.R. Hawke, Remote sensing of lunar pyroclastic mantling deposits, *Icarus*, 61, 461-489, 1985.
- Guest, J. E., and P.D. Spudis, The Aristarchus impact event and the effects of target material, *Geology*, 12, 317-327, 1985.
- Hagfors, T. Remote probing of the Moon by infrared and microwave emissions and by radar, *Radio Science*, 5, 189-227, 1970.
- Hagfors, T., A study of the depolarization of lunar radar echoes, *Radio Science*, 5, 445-465, 1967.

- Hawke, B. R., C.A. Peterson, P.G. Lucey, G.J. Taylor, D.T. Blewett, B.A. Campbell, C.R. Coombs, and P.D. Spudis, Remote sensing studies of the terrain northwest of Humorum basin, *Geophys. Res. Letters*, 20, 419-422, 1993.
- Hawke, B. R., and J.F. Bell, Remote sensing studies of lunar dark-halo impact craters: Preliminary results and implications for early mare volcanism, *Proc. LPSC 12B*, 665-678, 1981.
- Head, J. W., and eight others, Lunar impact basins: New data for the western limb and far side (Orientale and South Pole-Aitken Basins) from the first Galileo flyby, *J. Geophys. Res.*, 98, 17,149-17,181, 1993.
- Horz, F., R. Grieve, G. Heiken, P. Spudis, and A. Binder, Lunar surface processes, in Lunar Sourcebook, Cambridge Press, New York, 1991,
- Johnson, J. R., S.M. Larson, and R.B. Singer, Remote sensing of potential lunar resources 1. Near-side compositional properties, *J. Geophys. Res.*, 96, 18,861-18,882, 1991.
- Lucey, P.G., G.J. Taylor, and E. Malaret, Abundance and distribution of iron on the Moon, *Science*, 268, 1150-1153, 1995.
- McEwen, A. S., M.S. Robinson, E.M. Eliason, P.G. Lucey, T.C. Duxbury, and P.D. Spudis, Clementine observations of the Aristarchus region of the Moon, *Science*, 266, 1858-1862, 1994,
- McGetchin, T. R., M. Settle, and J.W. Head, Radial thickness variation in impact crater ejects: Implications for lunar basin deposits, *Earth & Plan. Sci. Letters*, 20, 226-236, 1973.
- Melendrez, D. E., J.R. Johnson, S.M. Larson, and R.B. Singer, Remote sensing of potential lunar resources 2: High spatial resolution mapping of spectral reflectance ratios and implications for nearside mare TiO_2 content, *J. Geophys. Res.*, 99, 5601-5620, 1994.
- Moore, H. J., J.M. Boyce, G.G. Schaber, and D.H. Scott, Lunar remote sensing and measurements, USGS Prof. Paper 1046-B, 1980.
- Oberbeck, V.R., The role of ballistic erosion and sedimentation in lunar stratigraphy, *Geophys.*, 13, 337-362, 1975.

- Olhoeft, G. R., and D.W. Strangway, Dielectric properties of the first 100 m of the Moon, *Earth and Planetary Sci. Lett.*, 24, 394-404, 1975.
- Papike, J., L. Taylor, and S. Simon, Lunar minerals, in Lunar Sourcebook, Cambridge Press, New York, 1991.
- Pieters, C. M., and 11 others, Crustal diversity of the Moon: Compositional analyses of Galileo SS1 data, *J. Geophys. Res.*, 98, 17127-17148, 1993.
- Pieters, C., Mare basalts on the front side of the moon: A summary of spectral reflectance data, *Proc. LPSC 9th*, 2825-2849, 1978.
- Pollack, J. B., and L. Whitehill, A multiple-scattering model of the diffuse component of lunar radar echoes, *J. Geophys. Res.*, 77, 4289-4303, 1972.
- Schaber, G. G., T.W. Thompson, and S.H. Zisk, Lava flows in Mare Imbrium: An evaluation of anomalously low Earth-based radar reflectivity, *The Moon*, 13, 395-423, 1975.
- Shoemaker, E. M., and E. Morris, Size distribution of fragmental debris, in Surveyor Project Final Report, Part 2, *JPL Tech. Rep. 32-1265*, 86-102, 1968.
- Shorthill, R.W., Infrared atlas charts of the eclipsed Moon, *The Moon*, 7, 22-45, 1973.
- Stacy, N. J. S., High-resolution synthetic aperture radar observations of the Moon, PhD. Diss., Cornell Univ., 1993.
- Stratton, J.A. 1947, Electromagnetic Theory, John Wiley, New York.
- Thompson, T. W., High-resolution lunar radar map at 70-cm wavelength, *Earth, Moon and Planets*, 37, 59-70, 1987.
- Thompson, T. W., W.J. Roberts, W.K. Hartmann, R.W. Shorthill, and S.H. Zisk, Blocky craters: Implications about the lunar **mega-regolith**, *The Moon and Planets*, 21, 319-342, 1979.
- Thompson, T.W., High resolution lunar radar map at 7.5-m wavelength, *Icarus*, 36, 174-188, 1978.
- Thompson, T.W., Atlas of lunar radar maps at 70-cm wavelength, *The Moon*, 10, 51-85, 1974.
- Thompson, T.W., J.B. Pollack, M.J. Campbell, and B.T. O'Leary, Radar maps of the Moon at 70-cm wavelength and their interpretation, *Radio Science*, 5, 253-262, 1970.

- Tyler, G. L., Comparison of quasi-specular radar scatter from the Moon with surface parameters obtained from images, *Icarus*, 37, 29-45, 1979.
- Ulaby, F. T., T. Bengal, J. East, M.C. Dobson, J. Garvin, and D. Evans, Microwave dielectric spectrum of rocks, Rep. 23817-I-T, Univ. of Michigan Radiation lab, Ann Arbor, MI, 1988.
- Ulaby, F. T., R.K. Moore, and A.K. Fung, Microwave Remote Sensing, Addison-Wesley, Reading, MA, 1987.
- Whitaker, E. A., Lunar color boundaries and their relationship to topographic features: A preliminary survey, *The Moon*, 4,348-355, 1972.
- Wilhelms, D. E., The geologic history of the Moon, USGS Prof. Paper 1348, 1987.
- Zisk, S. H., C.A. Hodges, H.J. Moore, R.W. Shorthill, T.W. Thompson, E.A. Whitaker, and D.E. Wilhelms, The Aristarchus-Harbinger region of the Moon: Surface geology and history from recent remote-sensing observations, *The Moon*, 17,59-99, 1977.
- Zisk, S. H., G.H. Pettengill, and G.W. Catuna, High-resolution radar maps of the lunar surface at 3.8-cm wavelength, *The Moon*, 10, 17-50, 1974.

TABLE 1. Volumetric rock population (in number per cubic meter, with radius r in cm), radar incidence angles, 70-cm radar LR and LL backscatter coefficients, and calculated Mie surface scattering cross sections for the Surveyor lunar landing sites. Backscatter coefficients calculated for 10×10 km box surrounding each landing site. The Surveyor 6 site falls in the central data gap of the 70-cm map. The Mie cross sections assume only a surficial layer of rocks, with possible dielectric contrasts shown by the range in values (soil $\epsilon' = 3$, rock $\epsilon' = 5-7$; rock $\tan \delta$ had little effect over the range 0.004-0.025). See text for discussion of volume scattering cross section.

| Surveyor | Rock Population | Angle (deg) | $\sigma_o^{LR}, \sigma_o^{LL}$ (dB) | Mie σ_o (dB) |
|----------|-----------------|-------------|-------------------------------------|---------------------|
| 1 | 1400 $r^{4.1}$ | 43 | -21.6, -29.5 | -32, -28 |
| 3 | 2700 $r^{4.9}$ | 23 | -15.1, -28.2 | -34, -30 |
| 5 | 980 $r^{4.63}$ | 23 | -14.6, -28.1 | -40, -36 |
| 6 | 2200 $r^{4.52}$ | * | * | -35, -31 |
| 7 | 4100 $r^{3.82}$ | 42 | -13.8, -16.0 | -24, -20 |

TABLE 2. List of craters with low-return haloes in 70-cm radar data. List divided into those on highland and mare surfaces. Areas where the surrounding mare may fortuitously give the appearance of a halo are indicated.

| Crater | Location (Lat, Len) | Type of Anomaly |
|-----------------------------------|--------------------------------|--|
| <i>Mare Craters:</i> | | |
| Aristoteles | 50.4 N, 16.9 E | Mare Frigoris; halo darker than surrounds |
| Galle | 56.1 N, 21.9 E | Mare Frigoris; halo darker than surrounds |
| Peirce | 18.9 N, 53.4 E | Mare Crisium; halo darker than surrounds |
| PiCard | 15.2 N, 54.6 E | Mare Crisium; halo darker than surrounds |
| Piazzi-Smyth | 42.3 N, 3.5 W | small dark-haloed crater |
| Bessel | 22.4 N, 17.9 E | Low-return oblong area which splits into two lobes |
| Delisle/Diophantus | 29.8 N, 34.6 W; 27.4 N, 34.1 W | Low-return area surrounds both craters |
| Krafft/Cardanus | 16.3 N, 72.7 W; 13.1 N, 72.5 W | Low-return arc to west of both craters |
| Galilaei and Galilaei A | 11.0 N, 63.0 W | Small dark halo surrounds both craters |
| Reiner | 6.8 N, 54.9 W | Oblong dark halo oriented NW-SE |
| Bullialdus | 21.0 S, 22.8 W | Slight darkening around crater |
| Taurantius | 6.0 N, 46.4 E | Very weakly defined halo |
| Aristillus | 33.9 N, 1.0 E | Surrounded by dark mare; may be fortuitous |
| Timocharis | 26.8 N, 13.5 W | Surrounded by dark mare; maybe fortuitous |
| Briggs/Russell | 26.5 N, 69.3 W; 28.0 N, 71.0 W | Surrounded by dark mare; may be fortuitous |
| Burg | 45.6 N, 27.9 E | Lacus Mortis; "halo" identification uncertain |
| <i>Mixed or Highland Craters:</i> | | |
| Hercules/Atlas | 41.4 N, 47.2 E | Appear to have mixed mare into highlands nearby |
| Plato | 51.7 N, 9.8 W | Surrounded by low-return areas in the Jura Mts. |
| Aristarchus | 23.6 N, 47.6 W | Low-return wedge on highlands N and E of crater |
| Petavius | 25.0 S, 606.6 E | Radar dark ejects on surrounding highlands terrain |
| Theophilus | 10.9 S, 26.4 E | Low-return halo on mare side of target area only |
| Hainzel | 40.1 S, 34.5 W | Low-return halo in surrounding highlands |
| Schluter | 5.3 S, 83.4 W | Oblong dark halo in highlands |

Figure Captions

Fig. 1. 70-cm wavelength depolarized radar map of the Moon, from Thompson [1987], Orthographic projection; image resolution 3-5 km. Mare sample boxes discussed in text are noted in white. Four of these boxes are near the northwest limb in Oceanus Procellarum, and one is located along the western limb by the crater Cardanus.

Fig. 2. Lunar mean LR back scatter coefficient vs. Hagfors scattering function with rms slope of 2° , surface reflectivity 7%. Hagfors model shown by dotted line, lunar mean shown by solid line. Note that the quasi-specular model underestimates the mean backscatter by a significant amount.

Fig. 3. Change in backscatter cross section for a buried substrate as a function of layer depth and loss tangent for an incidence angle of 45° , Depth of regolith chosen to be 3, 5, and 8 m. Note that the dynamic range of substrate echoes for regolith depths >5 m over the possible loss tangent range is at least 10 dB, compared to the 8 dB range actually observed across the maria.

Fig. 4. Volume scattering results based on Surveyor 111 rock population. Depth of the scattering layer is assumed to be 5 m (solid lines) and infinity (dotted lines). The higher backscatter values correspond to a rock/soil dielectric contrast of 4, while the lower values for each depth correspond to a contrast of 2.

Fig. 5. Circular polarization ratios (LL/LR) for five Hawaiian lava flows at 68-cm wavelength as a function of incidence angle. These flows span the range from very rough a'a (highest ratios) to smooth pavement-like pahoehoe texture (lowest ratios). Numbers noted next to each curve correspond to site locations and unit descriptions from [Campbell et al., 1993; Figure 2]. The rougher flows have widely varying polarization ratios. Stars indicate values for the mare sample sites noted in Figure 1.

Fig. 6. (a) 70-cm LR echoes vs. incidence angle, with stars to indicate mare sample sites; (b) 70-cm LL echoes vs. incidence angle, with stars to indicate mare sample sites. Lunar mean backscatter value shown by solid line. Plot symbols denote backscatter coefficients for five

Hawaiian lava flows from the AIRSAR 68-cm system, with site numbers as discussed for Figure 5.

Fig. 7. Enhancements in LL and LR radar cross sections, relative to the lunar mean value, for the mare sample sites. Note the close correlation between the two enhancements.

Fig. 8. 70-cm LR echoes, corrected for the $\cos\phi$ effect of projected area, vs. TiO_2 values from Johnson et al. [1991] (filled squares) and FeO values from Lucey et al. [1995] (open squares).

Fig. 9. The Mare Fecunditatis area, showing the low 70-cm radar returns from the mare basalts and in a halo around Petavius crater (PE). Langrenus crater also indicated (LA). (a) 70-cm depolarized radar image. Sinusoidal projection of the area 10°N -400 S, 35-850 E. (b) USGS shaded relief map of the identical area.

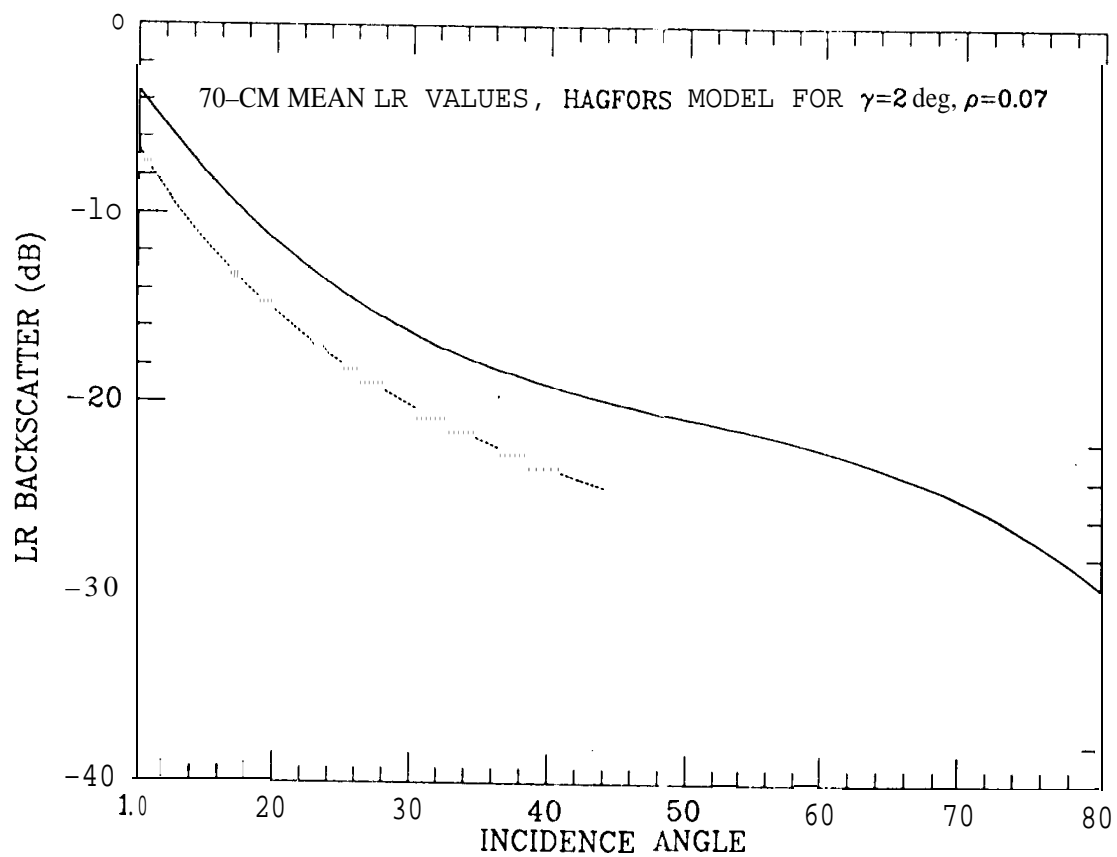
Fig. 10. Plot of radar power loss (in dB) due to mare contamination of a highlands soil for three mare material loss tangent values (0.002, 0.010, 0.020).

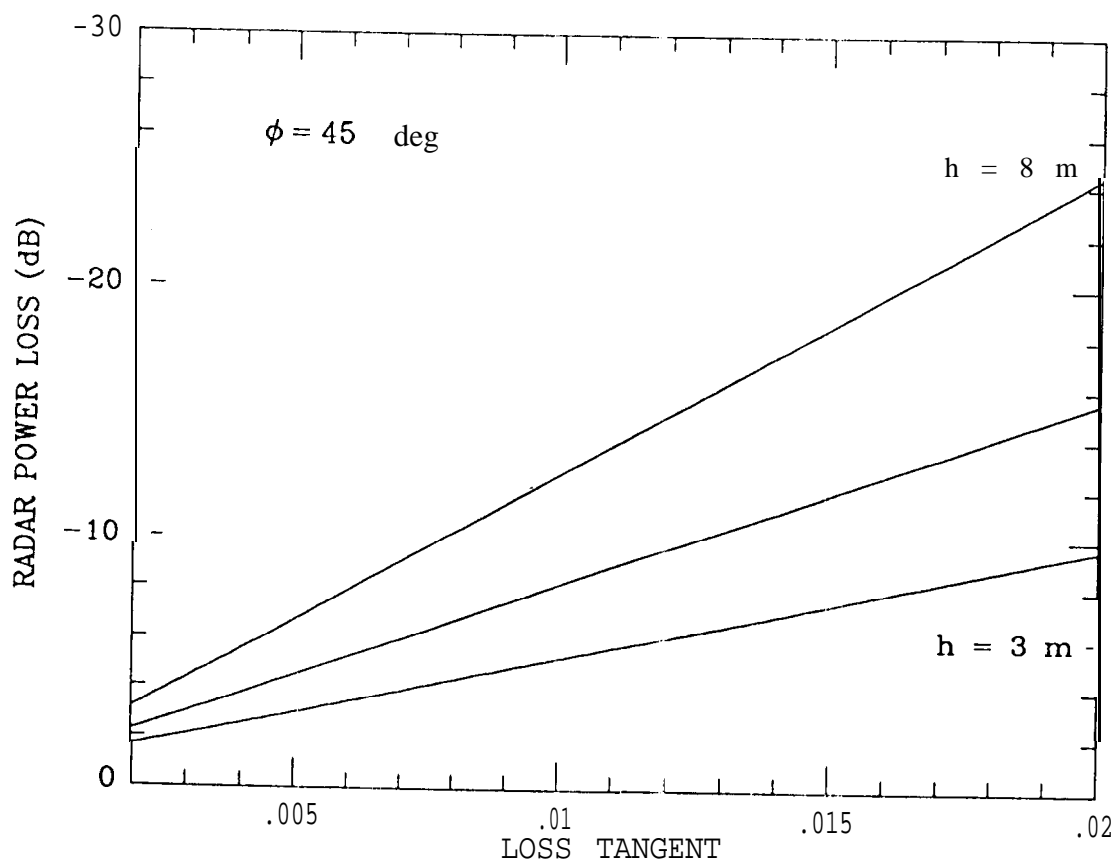
Fig. 11. Plot of radar power loss (in dB) due to a mantle of rock-free soil on a normal regolith layer for three loss tangent values (0.002, 0.010, 0.020).

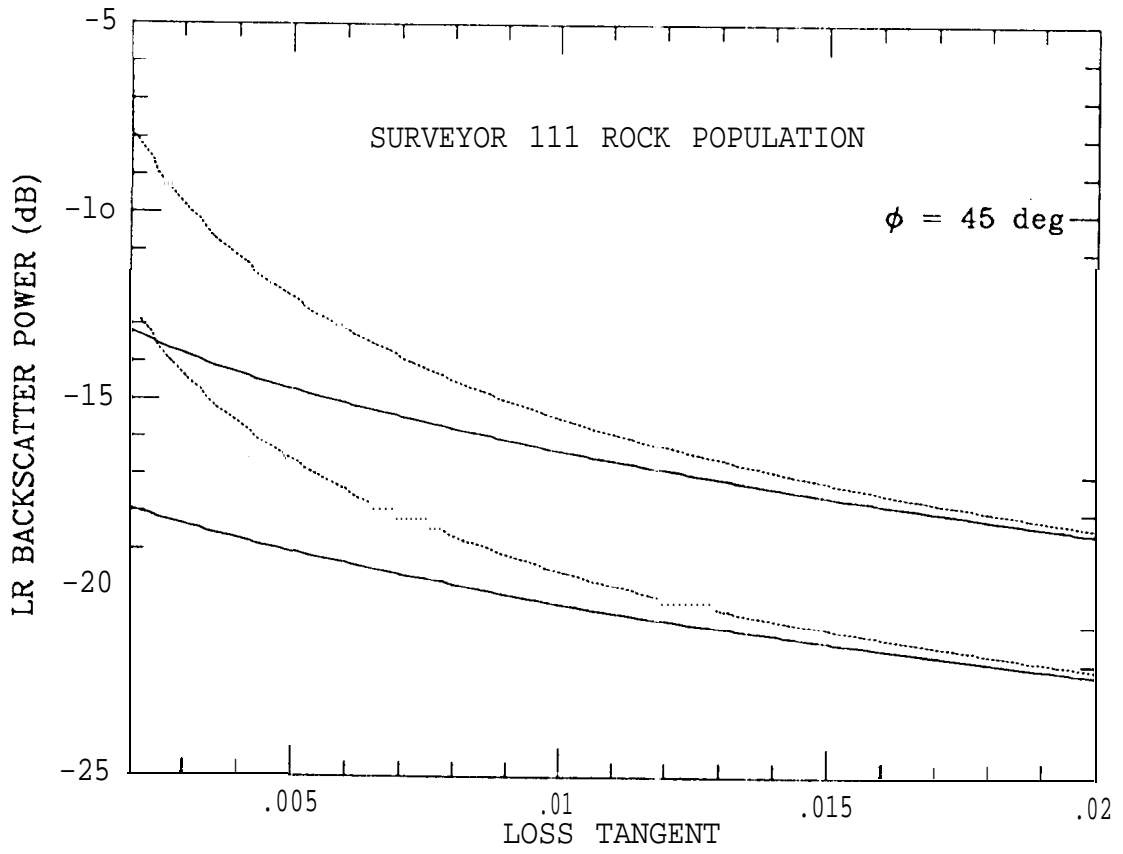
Fig. 12. The Mare Humororum area, showing the low 70-cm radar returns associated with the highland regions west and northwest of Gassendi crater. (a) 70-cm depolarized radar image. Sinusoidal projection of the area 7-350 S, 26-540 W. (b) USGS shaded relief map of the identical area.

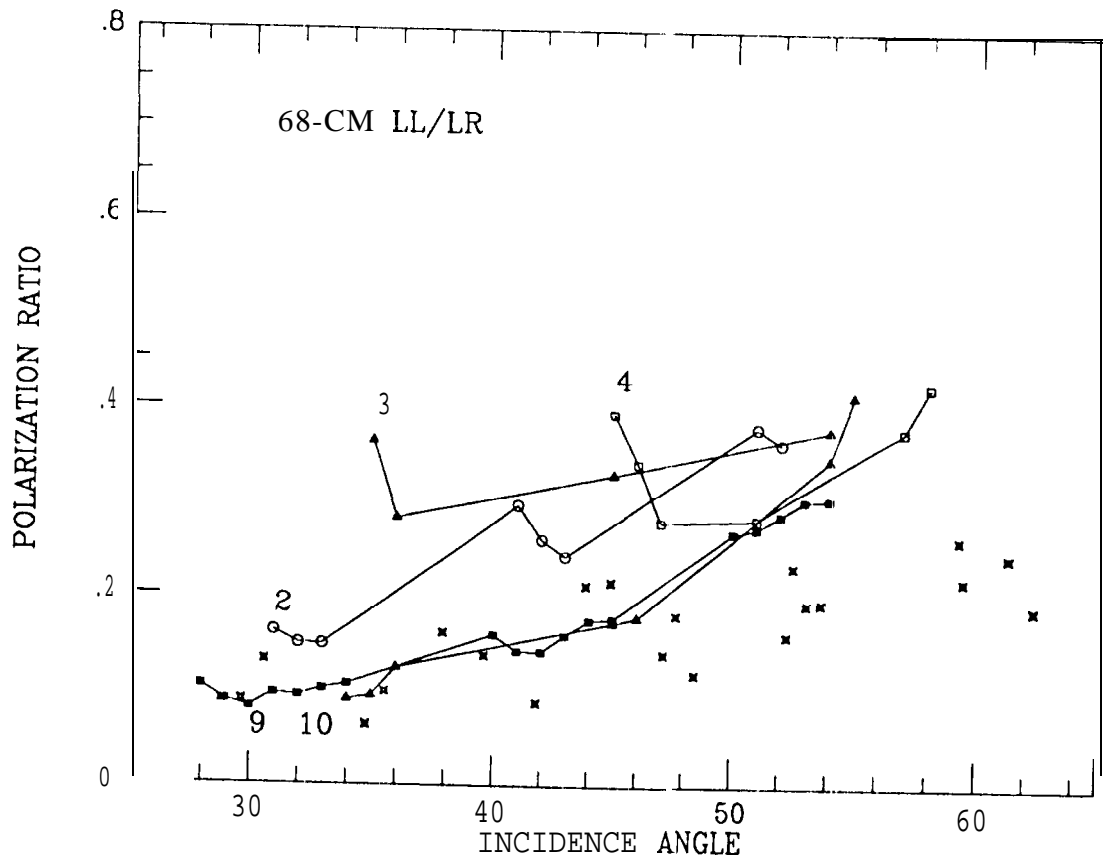
Fig. 13. 7.5-m radar image of the Moon, from Thompson [1978], as a color overlay to the USGS shaded-relief map. Orthographic projection; image resolution 30-50 km. Colors show logarithmic scaling of backscattered power.

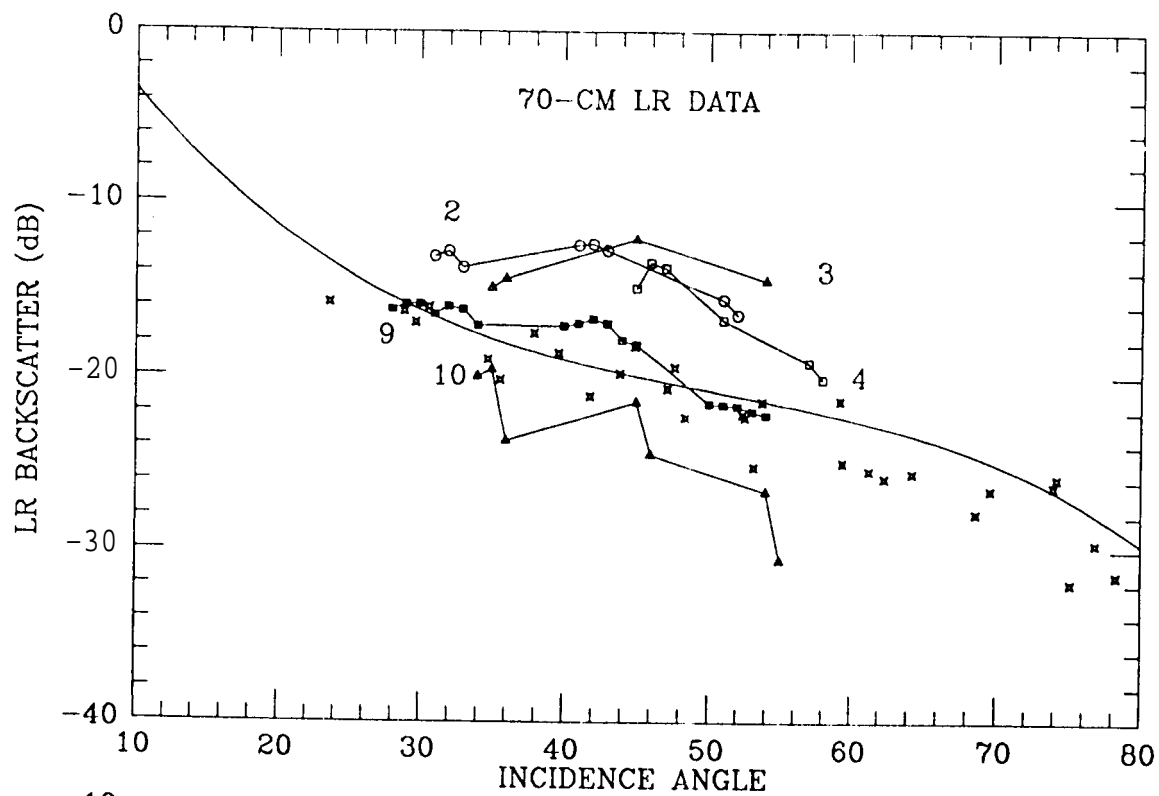




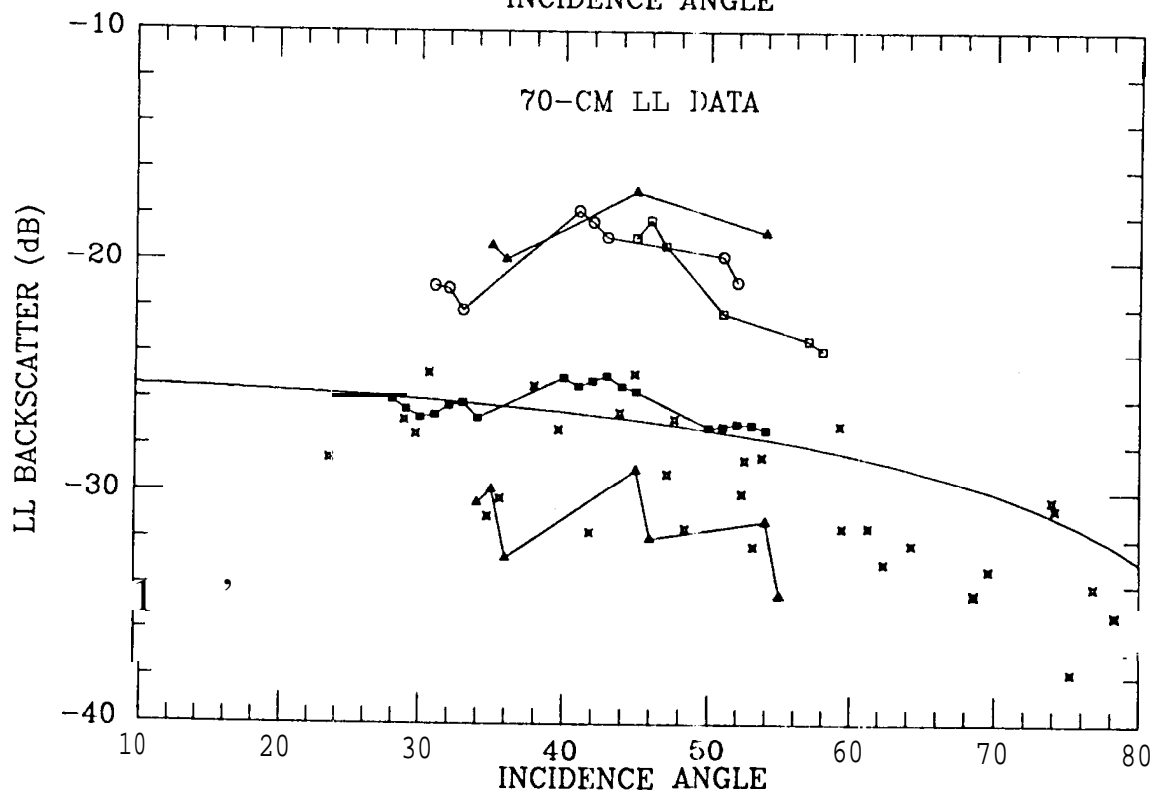




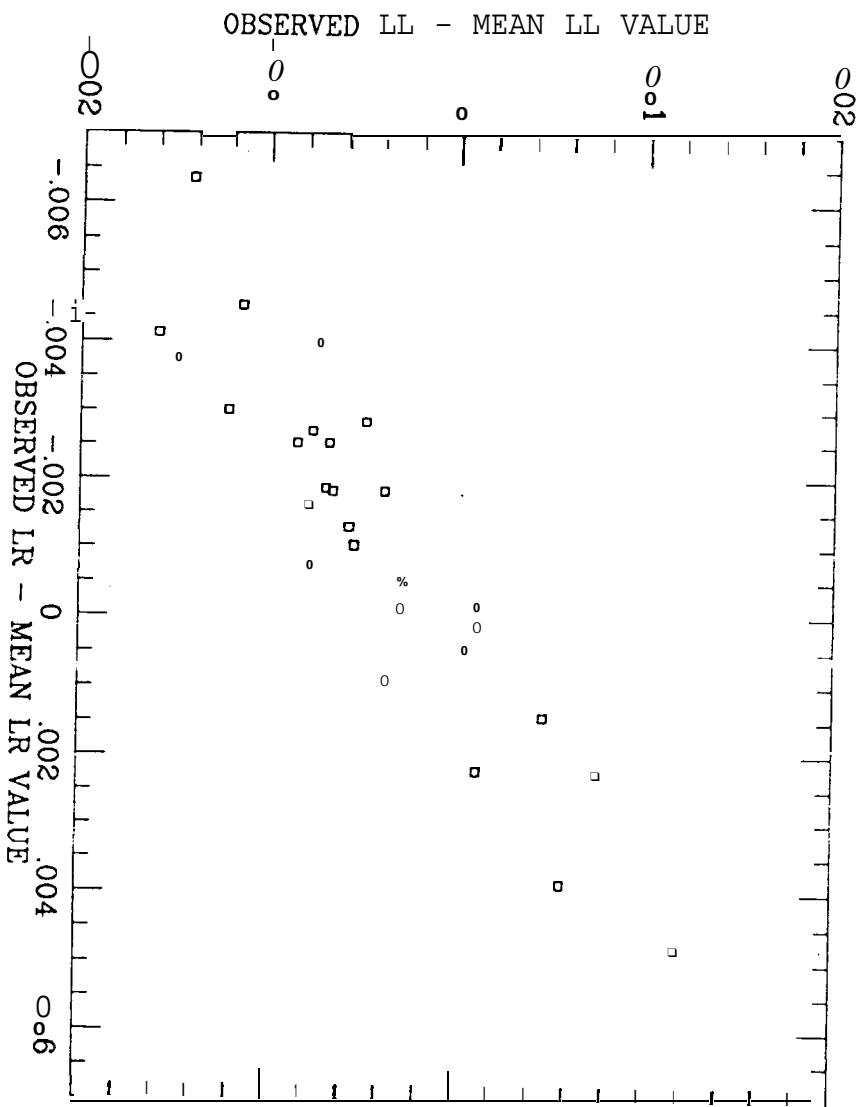


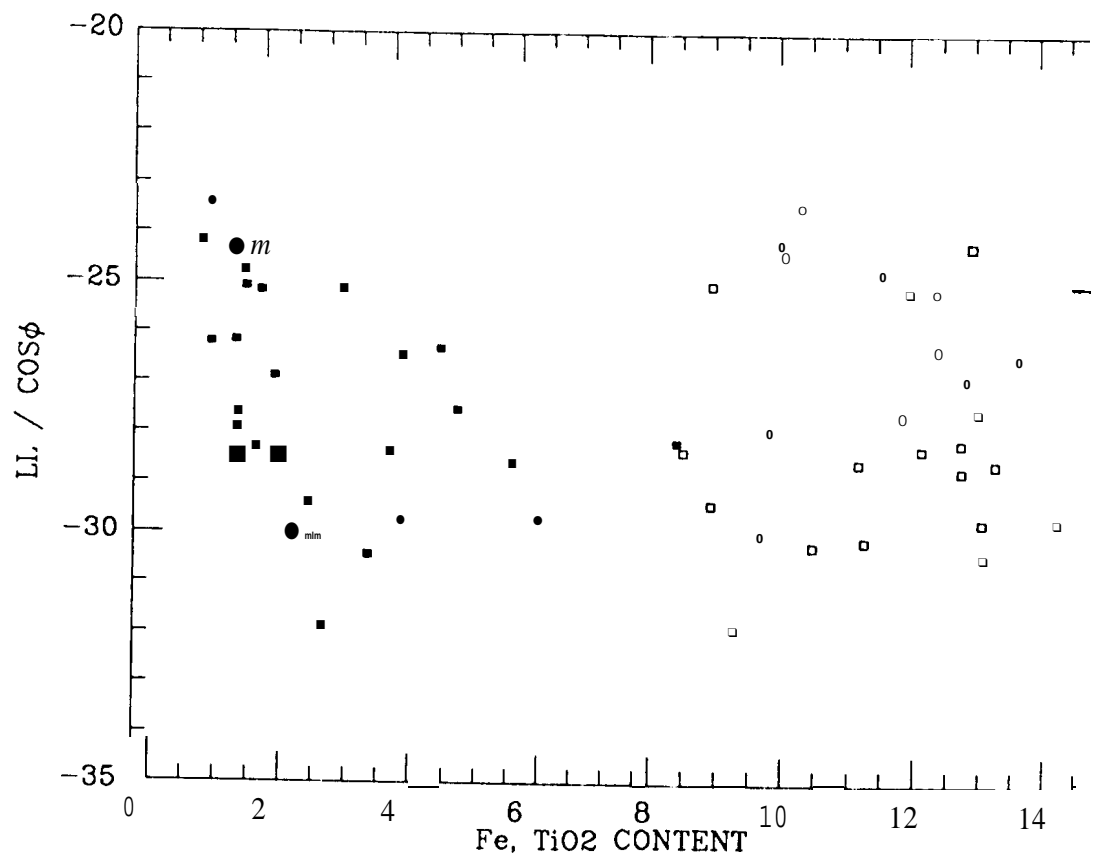


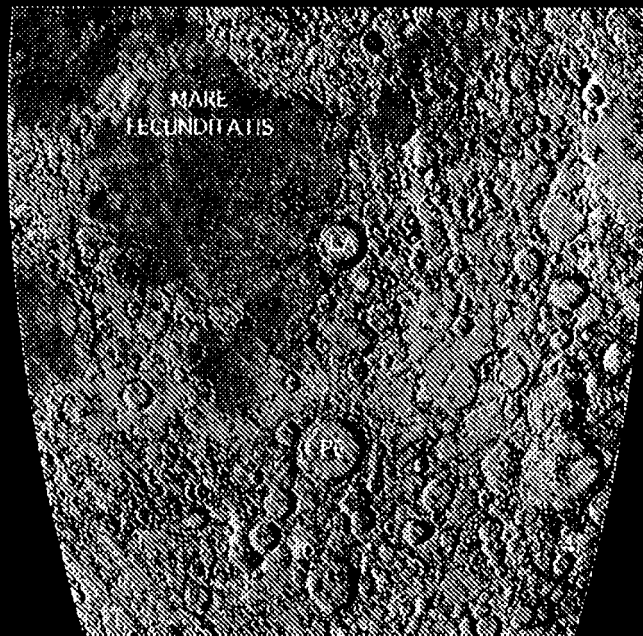
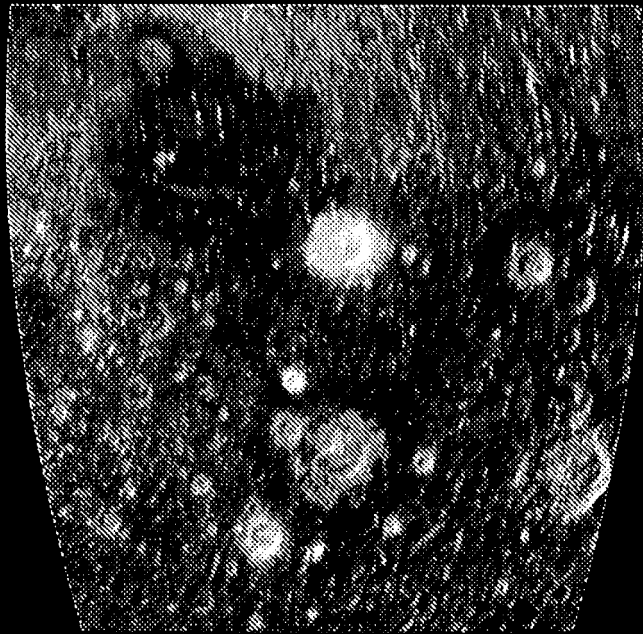
A

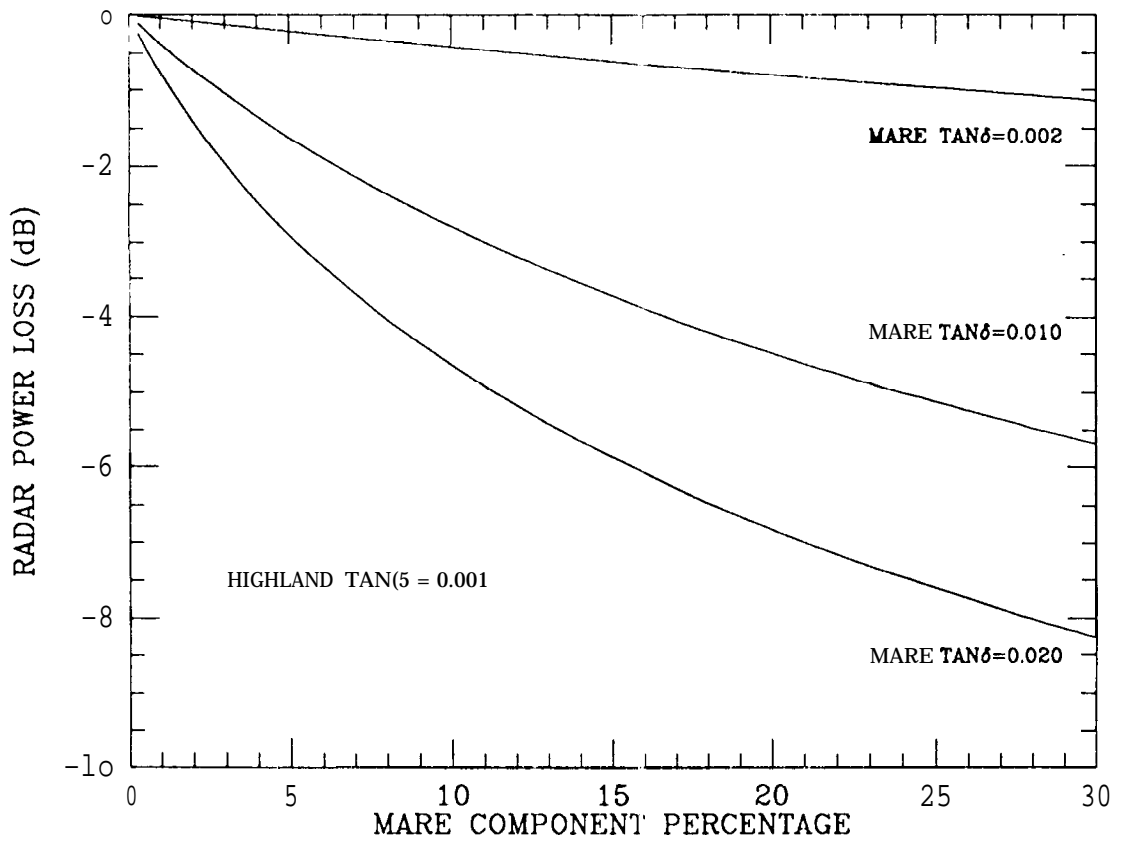


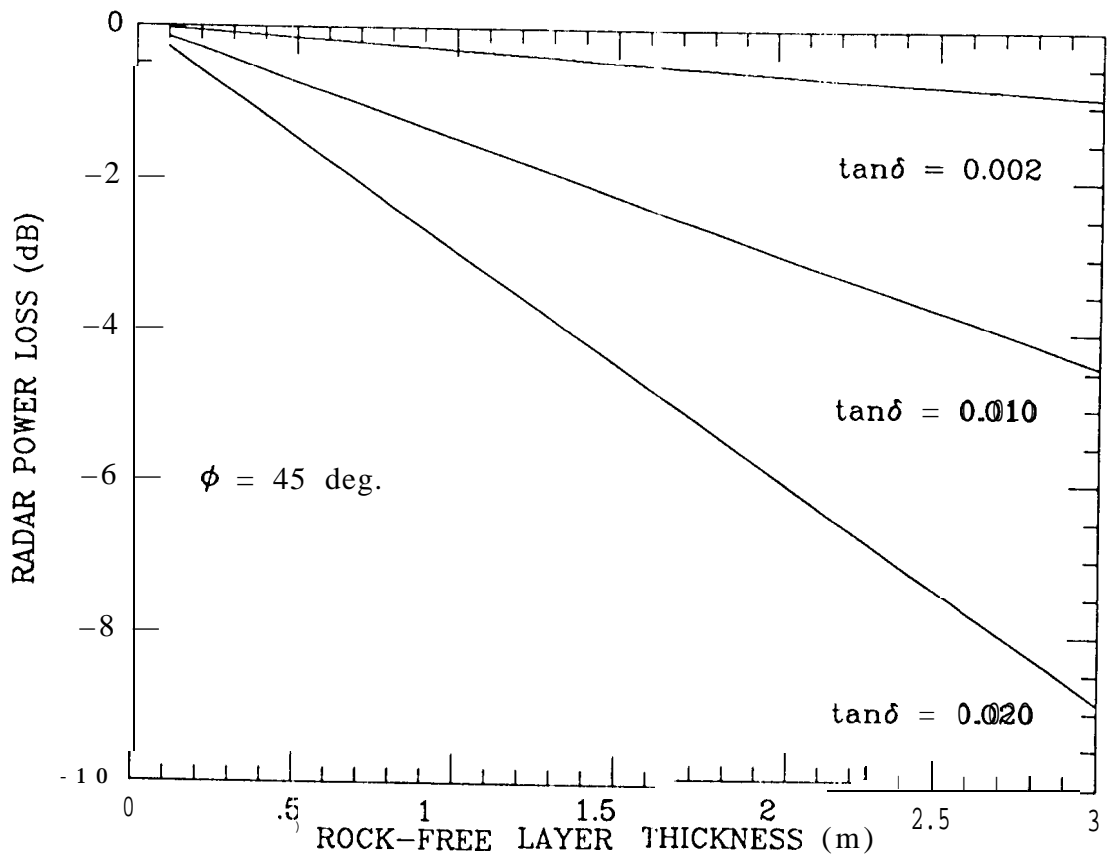
B

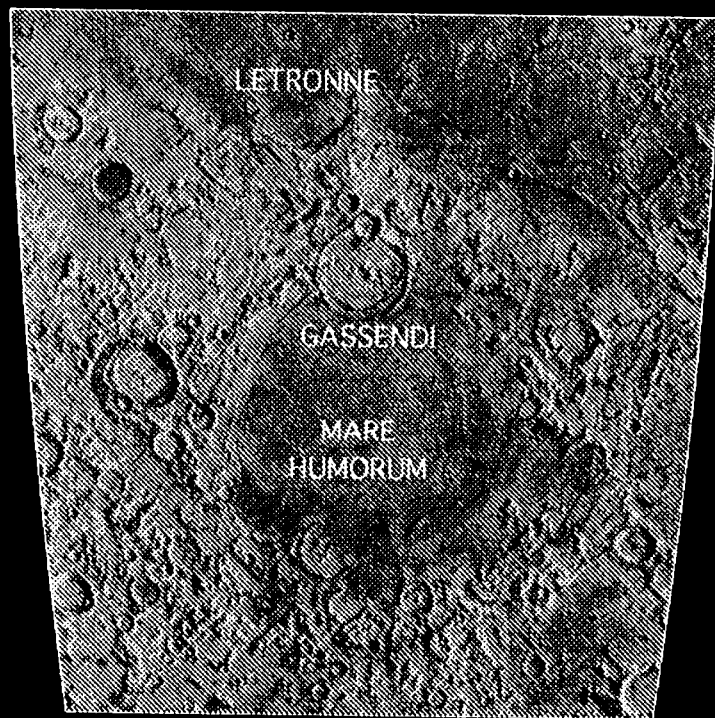
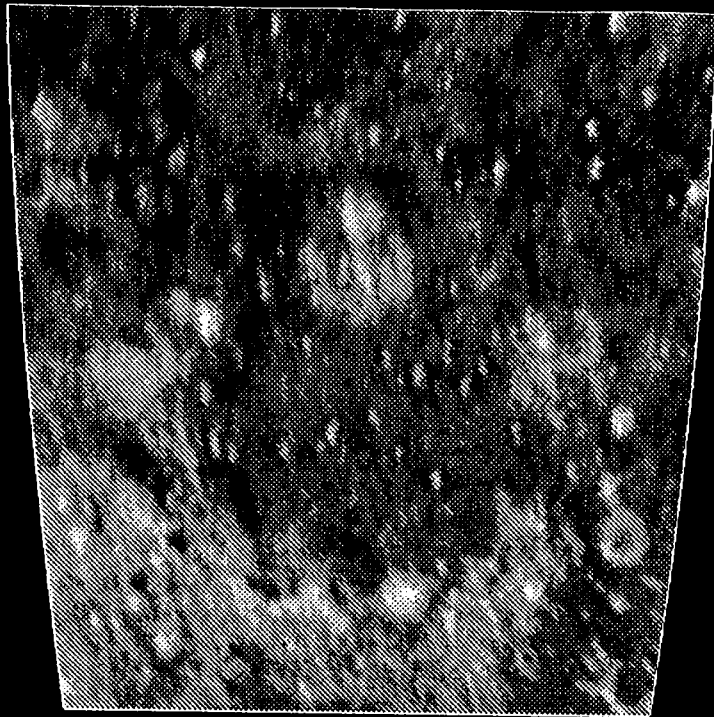


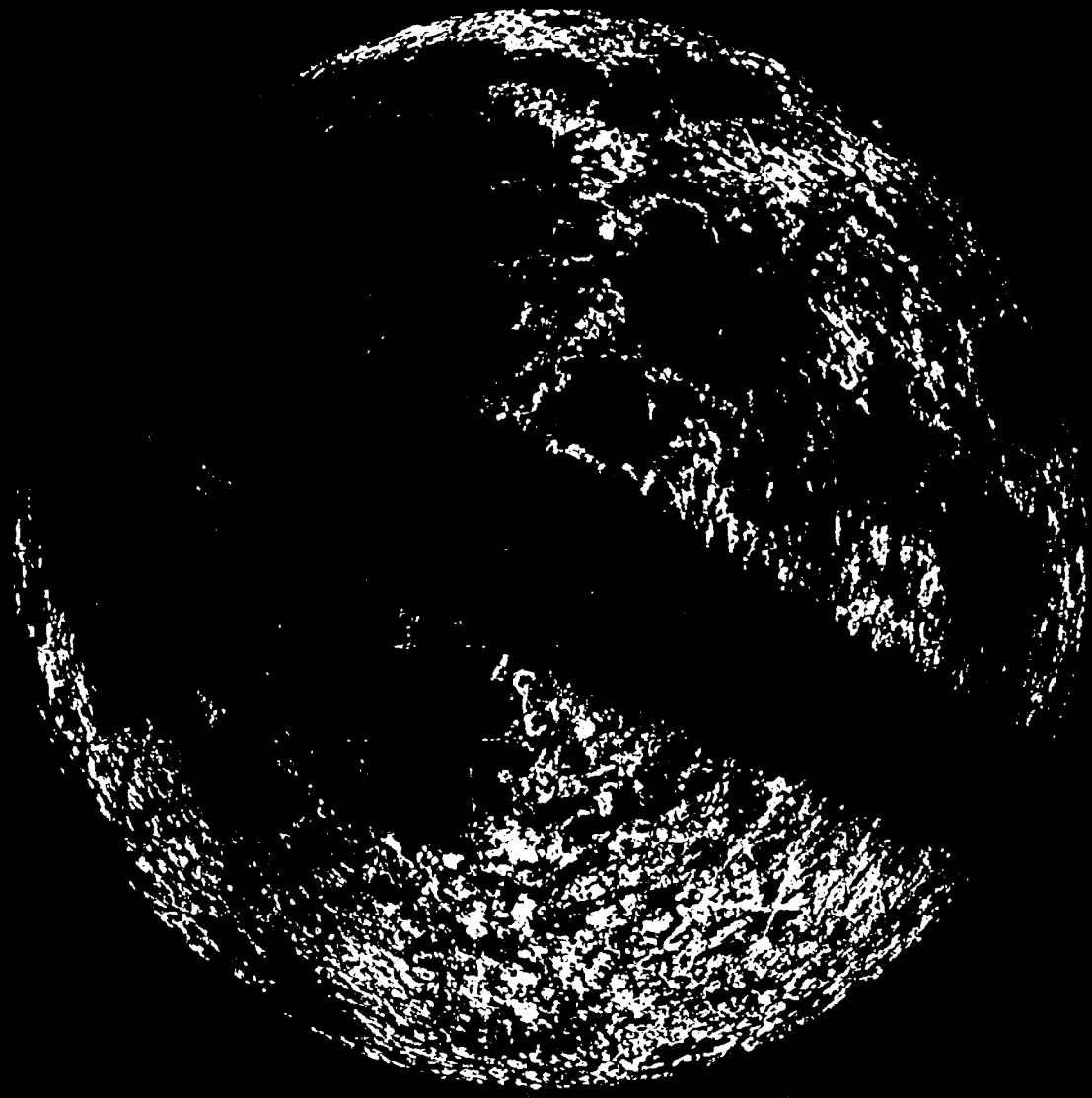












7.5-M LR BACKSCATTER COEFFICIENT